Published in final edited form as:
J Immunol. 2016 September 1; 197(5): 1957–1967. doi:10.4049/jimmunol.1500686.

Bimodal expansion of the lymphatic vessels is regulated by the sequential expression of IL-7 and LT α1β2 in newly formed tertiary lymphoid structures

Saba Nayar[1], **Joana Campos**[1], **Ming May Chung**[1], **Leyre Navarro-Núñez**[3], **Menka Chachlani**[1], **Nathalie Steinthal**[1], **David H Gardner**[1], **Philip Rankin**[1], **Thomas Cloake**[1], **Jorge H Caamaño**[3], **Helen M McGettrick**[1], **Steve P Watson**[2], **Sanjiv Luther**[4], **Christopher D Buckley**[1], and **Francesca Barone**[1]

[1]Rheumatology Research Group, Centre for Translational Inflammation Research, Institute of inflammation and Ageing, University of Birmingham Research Laboratories, Queen Elizabeth Hospital, Birmingham, B15 2WD, UK [2]Cardiovascular Sciences, College of Medical & Dental Sciences, University of Birmingham [3]MRC Centre for Immune Regulation College of Medical & Dental Sciences, University of Birmingham, B15 2TT, UK [4]Department of biochemistry, University of Lausanne, Switzerland

Abstract

Lymphangiogenesis associated with tertiary lymphoid structure (TLS) has been reported in numerous studies. However, the kinetics and dynamic changes occurring to the lymphatic vascular network during TLS development have not been studied. Using a viral-induced, resolving model of TLS formation in the salivary glands of adult mice we demonstrate that the expansion of the lymphatic vascular network is tightly regulated. Lymphatic vessels expansion occurs in two distinct phases. The first wave of expansion is dependent on IL-7. The second phase, responsible for leucocyte exit from the glands is regulated by LTβR signalling. These findings, while highlighting the tight regulation of the lymphatic response to inflammation, suggest that targeting the $LT\alpha_1\beta_2$/LTβR pathway in TLS associated pathologies might impair a natural pro-resolving mechanism for lymphocyte exit from the tissues and account for the failure of therapeutic strategies that target these molecules in diseases such as rheumatoid arthritis.

Introduction

During inflammation or following immunization critical changes occur to the non-hematopoietic stromal component (fibroblast subsets, blood and lymphatic endothelial cells) of the target tissue. Lymph node swelling occurs as a result of active stromal cell proliferation, accumulation of follicular dendritic cells (FDC) and the expansion and stretching of fibroblastic reticular cells (FRC), due to mechanical changes that occur to the FRC cell cytoplasm (1). Similarly, changes in the vascular system occur upon immunization

Corresponding author: Dr. Francesca Barone, MD, PhD, ARUK Senior Fellows, Senior Lecturer, Rheumatology Research Group, Centre for Translational Inflammation Research, Institute of Inflammation and Ageing, University of Birmingham Research Laboratories, Queen Elizabeth Hospital, Birmingham, B15 2WB, Direct Line: +44 (0)121 371 3248, f.barone@bham.ac.uk.

Europe PMC Funders Author Manuscripts

that allow a dramatic expansion of the lymphatic and vascular network which enables maximal cellular interaction and increases cellular output from the lymph node (2). The enlargement of the pre-existing lymphatic network is achieved by *de novo* formation of lymphatic vessels, also known as lymphangiogenesis (3–7). The cytokine IL-7 produced both by FRC and by lymphatic endothelial cells has been shown to contribute to this phenomenon during lymph node remodeling in a paracrine and autocrine manner (8) (9). $LT\alpha_1\beta_2$/LTβ Receptor (LTβR) signalling is believed to contribute to the homeostatic regulation of the lymphatic vessels in secondary lymphoid organs (SLOs) (10). Interestingly, $LT\alpha_1\beta_2$ signalling is also responsible for the formation and maintenance of fibroblast network, which in turn produces cytokines critical to preserve vascular integrity, such as VEGF-A and -C (11, 12). We have recently shown how defects in lymphatic vessel formation in the lymph node anlagen profoundly impair development and function of these organs (13). Similarly, in adult life, interruption of lymphatic vessels is known to impair lymph node homeostasis (14), thus highlighting the reciprocal relationships that take place between vascular cells, the lymphatic system and lymphoid fibroblastic cells in SLOs.

Tertiary lymphoid structures (TLS) are ectopic accumulations of lymphoid cells within peripheral tissue that share many cellular compartments, spatial organization, vasculature, chemokines and function with SLOs. TLS form preferentially at mucosal sites in response to chronic antigenic challenge during infections or autoimmune diseases (i.e. in the salivary glands of patients with Sjogren's syndrome or in the thyroid glands of patients with Hashimoto's disease) (15–18). We and others have described the formation of activated stromal cell networks within TLS with the concomitant expression of lymphoid chemokines and cytokines (such as $LT\alpha_1\beta_2$) that regulate lymphocyte clustering and organization (19, 20). TLS formation recapitulates some aspects of embryological SLO development. Moreover, Rorγt+ lymphoid tissue inducer (LTi) cells and activated stromal cells have been identified at these sites (16, 21–26). Although mechanisms leading to lymphangiogenesis in lymph nodes are relatively well understood, there is still limited information regarding the signals that regulate inflammatory lymphangiogenesis within TLS. Using a recently described, inducible model of TLS formation (27), we have dissected the expansion of the lymphatic vascular network within ectopic lymphoid organs that form in the salivary glands. We have observed expansion of lymphatic endothelial cells (LECs) compartment and an increase in number of lymphatic vessels. This expansion, synchronous with the development of the inflammatory aggregates, results in progressive vascular splitting and is dependent on the presence of IL-7, LTα1β2 and infiltrating lymphocytes, in a similar manner to what observed in SLOs. In our resolving model, this enlarged lymphatic system sustains the lymphocyte egress from the tissue, suggesting that in TLS-associated diseases targeting the lymphotoxin pathway might be counterproductive for the resolution of the lymphoid cell aggregates.

Materials and Methods

Mice and salivary gland cannulation

C57BL/6 mice were from Harlan. *Ltβr-/-* mice, R*orc-/-* mice, *rag2-/-* mice (on *boyJ* background) and *boyJ* mice were bred in the Biomedical Service Unit at the University of

Birmingham. All mice were maintained under specific pathogen-free conditions in the Biomedical Service Unit at the University of Birmingham according to Home Office and local ethics committee regulations. Under ketamine/domitor anesthesia, the submandibular glands of female C57BL/6, *boyJ* and knock-out mice (8-12 weeks old) were intraductally cannulated with 10^8-10^9 plaque forming units (pfu) of luciferase-encoding replication-defective adenovirus (Adv5), as previously described15. Animals were recovered from anaesthesia. Mice were culled by terminal anaesthesia at day 2, 5, 8, 15, 23 or day 26 post cannulation and salivary glands were harvested.

In vivo Blocking with anti-IL-7Rα

Rat anti-mouse anti IL-7Rα Ab was used as described (28). Starting at either day 0 p.c., mice were administered a dose of 100 μg of antibody via i.p injection followed by daily injections for four days.

In vivo treatmet of *ltβR-/-* with recombinant VEGF-C

Recombinant VEGF-C (Abcam) was administrated in the salivary glands of *Ltβr-/-* mice at the dose of 2 micrograms/ gland, at day 6 p.c., mice were sacrificed at day 8 and glands were analysed.

Histology and Immunofluorescence

Salivary glands from virus or control vehicle cannulated mice were harvested and snap frozen in OCT over liquid nitrogen. Frozen sections of 6μm in thickness were cut, left to dry overnight at room temperature, and stored next day in -80°C until use. For immunofluorescence analysis, slides were allowed to come to room temperature and then fixed for 20 mins in ice-cold acetone, left to dry and then hydrated in PBS. For immunofluorescence staining, all dilutions of reagents and antibodies were made in PBS with 1% BSA. Firstly, to block endogenous biotin, sections were treated with 0.05% avidin and 0.005% biotin for 15 mins each and washed for 5 mins with PBS in between the two incubations, followed by, blocking with 10% horse serum for 10 minutes. Slides were then incubated for 60 minutes with ‘cocktails’ containing the following primary antibodies in PBS (1% BSA); gp38/podoplanin clone 8.1.1, CD4 Alexa Fluor 647 or CD4 Pacific Blue clone RM4-5 (from BD Pharmingen), CD31-biotin or CD31-FITC clone 390, CD19 Alexa Fluor647 clone eBio1D3, CD3e biotin clone ebio500A2 and RORgamma(t) clone AFKJS-9 (all were from ebiosciences) and CCL21 (goat polyclonal). CD31 FITC-conjugated antibodies were detected using rabbit anti-FITC (Sigma-Aldrich), then goat anti-rabbit IgG-FITC (Jackson ImmunoResearch Laboratories, West Grove, PA). CCL21 antibodies were detected using donkey anti-goat FITC (Jackson ImmunoResearch Laboratories) then rabbit anti-FITC (Sigma-Aldrich), followed by goat anti-rabbit IgG-FITC (Jackson ImmunoResearch Laboratories, West Grove, PA). RORgamma(t) were detected with goat anti-rat FITC (Southern Biotech) then rabbit anti-FITC (Sigma-Aldrich), followed by goat anti-rabbit IgG-FITC (Jackson ImmunoResearch Laboratories, West Grove, PA). gp38/podoplanin was detected using goat anti-hamster biotin (Cambridge Bioscience, Cambridge, U.K.). Biotinylated antibodies were detected using streptavidin-Alexa Fluor 555 or 488 (Molecular Probes). Hoescht (Molecular Probes) was used for nuclear stain. All secondary

antibodies were incubated for 30 minutes. Slides were mounted with Prolong Gold Antifade reagent (Invitrogen Life Technologies).

Images were acquired on a Zeiss LSM 510 laser scanning confocal head with a Zeiss Axio Imager Z1 microscope. Digital images were recorded in four separately scanned channels with no overlap in detection of emissions from the respective fluorochromes. Confocal micrographs were stored as digital arrays of 2048×2048 pixels with 8-bit sensitivity; detectors were routinely set so that intensities in each channel spanned the 0-255 scale optimally. The LSM510 Image Examiner Software was used to process these images.

Lymphatic Quantitation

In order to investigate the dynamics of lymphatic vessels during different phases of the inflammatory process in inflamed salivary glands we stained for the lymphatics using LYVE-1 antibody (Abcam) and imaged the whole tissue section using the Leica DM6000 (as mentioned above). Using the ImageJ software, we drew a region around the lymphatic vessels and estimated both the area covered by the lymphatic vessels and the total tissue area. This data was then used to calculate the size of lymphatic vessels as relative area covered by lymphatic vessels (%). We also counted the lymphatics in each tissue section to ascertain the number of lymphatics per area of tissue. Analysis was performed by 2 blinded observers.

Isolation of stromal cells

Harvested salivary glands from virus or vehicle control cannulated mice were cut into small pieces and digested for 40 min at 37°C with gentle stirring in 1.5 ml RPMI 1640 medium containing collagenase D (3.7 mg/ml; from Roche), DNAse I (30ug/ml; from Sigma) and 2% (vol/vol) FCS. The suspension was gently pipetted at 15 min intervals to break up aggregates. The remaining fragments were further digested for 20 min at 37 °C with medium containing collagenase dispase (3.7 mg/ml) and DNAse I (30ug/ml). The suspension was then gently pipetted to break up remaining aggregates until no visible fragments remained. During the final pipetting, EDTA was added to a final concentration of 5 mM to further reduce cell aggregates. Cells were then passed through a 70-μm mesh, were washed twice and were resuspended in RPMI 1640 medium containing 10% (vol/vol) FCS.

Flow cytometry

Single cells suspensions were stained for 30 minutes in PBS (with 0.5% BSA and 2mM EDTA) with ‘cocktails’ of the following antibodies CD31-FITC clone 390, gp38-PE clone 8.1.1, CD45 PerCP/CY5.5 clone 30-F11 (from eBiosciences), EPCAM PE/Cy7 clone G8.8 (from Biolegend), Ki67-Alexa 647 and BrDU-Alexa647 (BD Pharmingen). Afterwards cells were washed twice, re-suspended and then analyzed using a Cyan-ADP (Dako) with forward/side scatter gates set to exclude non-viable cells. Data were analyzed with FlowJo software (Tree Star).

In vitro tube formation assay

The tube formation assay was performed on 12-well plates coated with 100 μl Matrigel (BD Biosciences, Oxford, UK) as previously described with modifications (1). After

polymerization of matrigel at 37°C for 30 min, human lymphatic endothelial cells (HLECs, 1.5 x 10^5 cells per well) resuspended in 2 ml of MV2 growth medium (Promocell, Heidelberg, Germany) were seeded to each well and incubated at 37°C, 5% CO_2 for 1 hour. The medium was then changed and treatments added to the cells. 20% fetal calf serum (FCS) was used as a positive control. Recombinant Lymphotoxin (LT) α1β2 (R&D Systems Europe Ltd., Abingdon UK) was used at 2 μg/mL.

The effect of the stated treatments on HLEC network formation was evaluated 5 hours after their addition. Images were digitally captured using a Zeiss 0.16 NA Plan-Neofluar 5x Ph1 lens on a Zeiss Axiovert 200 inverted high-end microscope (Welwyn Garden City, UK) and a Hamamatsu Orca 285 cooled digital camera using Slidebook software (Intelligent Imaging Innovations). Analysis of cellular networks was performed using Gilles Carpentier's Angiogenesis Analyzer for ImageJ, available online at http://image.bio.methods.free.fr/ImageJ/?Angiogenesis-Analyzer-for-ImageJ, by quantifying total branching length, number of junctions and number of meshes in 5 different images per well. Comparisons between non treated, FCS supplemented, and LTα1β2 treated samples were carried out using one way ANOVA test followed Bonferroni's post-test. Results shown are mean +/- SD from three independent experiments.

RNA isolation and quantitative PCR

Total RNA was isolated from salivary glands with an RNeasy mini kit (Qiagen) and the RNA was then reverse-transcribed using the High capacity reverse transcription cDNA synthesis kit (Applied Biosystems) according to the manufacturer's specifications. Reverse transcription was carried out on Techne 312 Thermal Cycler PCR machine. Quantitative RT-PCR (Applied Biosystems) was performed on cDNA samples for LTβ and VEGF-C mRNA expression. β-actin was used as an endogenous control. The primers and probes used were from Applied Biosystems. The quantitative real-time PCR was run in duplicates on a 384-well PCR plate (Applied Biosystems) and detected using an ABI PRISM 7900HT instrument. Results were analyzed with the Applied Biosystem's SDS software (SDS 2.3). We used the mean of two technical replicates (C_t values) to calculate the ΔC_t value. The C_t of the β-actin was subtracted from the target gene C_t value and the relative amount was calculated as $2^{-\Delta C}{}_t$. RQ values were calculated as $2^{-\Delta\Delta C}{}_t$ where $\Delta\Delta C$t is the difference between the ΔC_t values of cannulated salivary glands and the ΔC_t of non-cannulated salivary glands. In the methods it looked as if you always compare virus- versus vehicle control-cannulated mice. It did not come across that you had non-cannulated glands as controls. C_t values above 34 were not accepted, neither were technical replicates with more than two cycle differences between them.

Statistics analysis

Statistical analysis was determined for all analysis in figures (except figure 6) with student's t test. Statistical significance in figure 6 was determined by One-way ANOVA.

Results

Bimodal expansion of the lymphatic vascular network during TLS development

In order to dissect the dynamics of lymphatic vessel expansion in the context of ectopic lymphoneogenesis we used a model of TLS formation in the salivary glands, where the single administration of a replication deficient adenovirus via retrograde cannulation of submandibular glands is sufficient to induce focal aggregate formation as observed in human Sjogren's syndrome (29). This model is characterised by expansion of lymphoid aggregates, T/B cell segregation and lymphoid chemokine expression, which reaches a peak around day 15, post cannulation (p.c.) and undergoes resolution with complete lymphocyte clearance by day 30 p.c. (suppl. fig 1a). These aggregates are characterised by expansion of a gp38+/ Podoplanin+ fibroblast network, previously observed in human TLS (suppl. fig1b,(22)).

Salivary glands of wild type (wt) mice were cannulated with replication deficient adenovirus or vehicle control. Mice were sacrificed at specific time points p.c. and salivary glands isolated as described (29). Flow cytometry on digested single cell suspension to evaluate the expansion of lymphatic endothelial cells (LECs) within the EpCAM-CD45- compartment (fig 1a) revealed a bimodal pattern of expansion of the gp38+CD31+ LECs. The first peak coincided with the initial establishment of the TLS and was observed around day 5 to 8 p.c. (fig 1b). A second phase of expansion occurred after day 15 p.c. and coincided with the beginning of the involution of the inflammatory foci (fig 1b and suppl. fig 1b). Investigation of the proliferative status of the LECs, using BrdU incorporation, administered to the mice continuously from the day of the cannulation, revealed stable proliferation of this compartment between day 5 and day 23 p.c. (fig 1c). The proliferation observed in the LEC associates with a stepwise increase in vegfc transcript upon cannulation of the salivary glands (fig 1d).

Remodelling of the lymphatic vascular network during TLS formation

Immunofluorescence analysis performed on dissected salivary glands post cannulation allowed direct visualisation and quantification of the lymphatic network in the context of the lymphoid aggregates. A combination of CD31 and Lyve1 staining showed the presence of lymphatic vessels in the glands with a tendency to localise in the outer part of the follicular aggregates at the earliest disease phases of TLS assembly (fig 2a and b). At this stage the majority of the lymphatic vessels were characterized by enlargement of the vascular lumen and the presence of lymphocytes within the vessels (fig 2b). This phenomenon was less evident in the later phases of the disease (day 23 p.c.) that were characterised by lymphatic vessels of smaller calibre, essentially devoid of lymphocytes (suppl. fig 2).

Quantification of the area covered by the lymphatic network was achieved by using ImageJ analysis on whole-section tile scans (see methods). A significant increase in the total number of vessels/tissue area was observed in the early phases of the TLS formation (day 5 p.c.) as compared to resting conditions. This increased number of vessels remained stable over time, with a further significant increase observed at day 23 p.c. (fig 2c). The average vessel area measured showed that an increase in lymphatic vessel number was associated with a

reduction in the mean vessel lumen area, suggesting progressive splitting of the pre-existing vessels (fig 2d).

Lack of LTα1β2 affects lymphangiogenesis in TLS

LTβR signalling has been reported to play a key role in physiological lymphoneogenesis during SLO development (30, 31). In order to investigate the effects of this pathway in TLS-associated lymphangiogenesis, we cannulated *Ltβr* knockout mice (*Ltβr-/-*). Aggregates formed in *Ltβr-/-* mice but were characterised by reduced organization and diminished chemokine expression (data not shown). Accordingly, the dynamics of vascular expansion was altered in these animals. The first peak of LEC expansion in *Ltβr-/-* mice was similar to their wt counterparts. Conversely, from day 8 p.c. we observed a decrease in the percentage of the LECs in the *Ltβr-/-* that became significant at day 23 and 26 p.c. (fig 3a). Despite this defective expansion of the lymphatic network, the LEC from *Ltβr-/-* mice appeared to proliferate at the same rate compared to wt mice (fig 3b).

Image analysis of the cannulated salivary glands of *Ltβr-/-* mice demonstrated in the knockout mice a decrease in the number of the lymphatic vessels that reached significance at day 15 and 23 p.c. (fig 3c). This phenomenon was associated with a tendency in the *Ltβr-/-* mice to form lymphatic vessels with larger calibre as compared to the wt controls (fig 3d and e). All together these data suggest that LTβR mediated signals are involved in the induction of lymphangiogenesis within TLS. Indeed, expression of LTβR is detected on salivary gland LECs (fig 3f)

The early phase of lymphatic vessels remodelling is dependent on IL-7

Onder et al reported a critical role for IL-7 in lymphatic remodelling in SLOs. In our cannulation model, IL-7 expression is significantly increased and preceded the expansion of the lymphatic bed (fig 4a). Moreover, LECs specifically express IL-7Rα, thus displaying the machinery to respond to this homeostatic signal in vivo (fig 4b).

In order to investigate whether IL-7 was responsible for the first phase of expansion of the lymphatic bed, that is intact in the *Ltβr-/-* mice, we treated wt-cannulated mice with a blocking antibody against IL-7Rα (see methods). Treated mice display significant decrease in LECs (fig 4c and d) and average lymphatic vessel area (fig 4e and g) and a smaller number of lymphatic vessels (fig 4f and g) that did not reach significance. This defect appeared to be due to a significant reduction in the proliferating ability of the LECs (fig 4h).

$LT\alpha_1\beta_2$ induces the formation of complex lymphatic networks

Interestingly, VEGF-C mRNA transcripts were significantly decreased in *Ltβr-/-* (fig 5a), thus suggesting the possibility that the defect observed in the *Ltβr-/-* is sustained by a defect in VEGF-C induction. In order to test this hypothesis we treated cannulated *Ltβr-/-* mice with recombinant VEGF-C (fig 5b) and observed a partial compensation of the defective phenotype described in these mice. VEGF-C treated mice indeed display a significant increase in lymphatic vessels number accompanied by a decrease in the average vessel calibre (fig 5c), thus suggesting that while VEGF-C provides a positive signal to sustain vascular splitting, this doesn't completely explain the phenotype observed in the *LtβR-/-.*

In order to evaluate whether $LT\alpha_1\beta_2$ could alone influence TLS lymphangiogenesis we used an *in vitro* tube formation assay in vitro. Primary human lymphatic endothelial cells (HLECS) were treated with either FCS or $LT\alpha_1\beta_2$ (see methods) and a series of parameters were collected upon imagining of the cultures (fig 6). We observed no difference in proliferation, total branching length or segments length of the tubes formed by the non-treated, FCS control and the $LT\alpha_1\beta_2$ treated cells (fig 6a and b). On the contrary, we detected a significant increase both in the number of nodes (junctions) (fig 6c), and number of meshes (fig 6d and e) in the $LT\alpha_1\beta_2$ treated cells, similar to that induced in FCS (serum) treated positive control, as compared to non-treated samples. These data indicate that $LT\alpha_1\beta_2$ facilitates the formation of a more sophisticated lymphatic network and are consistent with the observed phenotype of failed lymphangiogenesis present in the *Ltβr-/-* mice.

Lymphatic vessel formation is influenced by the expression of LTα1β2 by Rorγ$^+$cells

It is known that Rorγt+ lymphoid tissue inducer (LTi) cells represent the earliest source of $LT\alpha_1\beta_2$ during physiological lymphoneogenesis (31, 32). In order to dissect the specific contribution of both these cellular component to TLS associated lymphangiogenesis we induced TLS formation in the salivary glands of R*orc-/-* that are characterised by a defect in both LTi and Th17 cells formation. As predicted, the defect observed in the *Ltβr-/-* mice was largely reproduced in the R*orc-/-* mice. In these mice we observed decreased LEC expansion as compared to wt (fig 7a). Moreover, we detected a significant increase in the average lymphatic vessel area and decreased number of vessels, suggesting a defect in lymphangiogenesis similar to that observed in the L*tβr-/-* mice (fig 7b, c and d). This phenotype was not attributable to a proliferative defect, as shown by BrdU incorporation (suppl. fig 3).

Lack of lymphocytes affects both phases of lymphatic vessel expansion

In adult SLOs lymphocytes can compensate for the absence of LTi in the production of $LT\alpha_1\beta_2$. Accordingly, cannulated *Rag2-/-* mice display a similar phenotype to the *Ltβr-/-* mice in the late phase of vascular expansion, accompanied by a significant defect in lymphangiogenesis even in the first wave of expansion, both in terms of LECs (fig 8a) and in the lymphatic vessel area and number, the latter only showing a non-significant reduction (fig 8b and c). IL-7 transcripts in *Rag2-/-* mice showed a significant decrease as compared to wt (suppl. fig 3).

Discussion

During inflammation, expansion of the lymphatic vascular network is required to drain local oedema, increase cellular output and deliver infiltrating immune cells and antigens to draining lymph nodes. In order to accomplish these tasks lymphatic vessels undergo dramatic changes in shape and size that enable the clearance of immune cells and pathogens from the affected tissue (33).

TLS are aberrant accumulations of lymphocytes that form preferentially within inflamed mucosal sites and acquire features and functions similar to lymphoid tissue. In many

diseases, TLS persistence is associated with worse disease outcome and, in some cases, development of lymphoid malignancies (15, 34, 35). In the lymph node, expansion of the lymphatic vascular network synchronises with the enlargement of the lymphoid stroma and the increase in the influx of lymphocytes in order to preserve tissue homeostasis (12, 33). In TLS it is believed that this drainage system is defective and that lymphocyte accumulation occurs as a result of insufficient the expansion of the lymphatic network. Indeed, failure to drain activated lymphocytes from the tissue might contribute to the persistence of tissue inflammation (36–38).

Here we study the complex phenomenon of lymphoneogenesis evaluating the expansion of the LEC, as well as the changes in shape and size of the lymphatic vessels by immunofluorescence. In this work we demonstrate that the increase in lymphatic vessels is initiated in the early phases of TLS development, but that this process is delayed and impaired when the aggregates reach full size and higher degree of organization. At this stage lymphoid aggregates are surrounded by lymphocytes engulfed in lymphatic vessels, thus suggesting a reduction in the ability of the vascular network to drain the recruited lymphocytes. Interestingly, this phenomenon is reversed in the resolution phase of the TLS when a second wave of lymphatic vessel expansion occurs, together with the formation of small calibre lymphatic vessels that contribute to tissue clearance.

In our model the expansion of the lymphatic vascular network is preceded by a significant increase in both IL-7 and $LT\alpha_1\beta_2$ expression within the tissue both known to regulate leucocyte homeostasis and lymphangiogenesis in SLOs (39, 40) (fig 4a and suppl. fig 4). IL-7 autocrine signal on the LECs in SLO has been shown to regulate lymphatic vessel remodelling and expansion(9). In addition, fibroblast derived IL-7 appear to support lymphangiogenesis in a paracrine manner (8), thus candidating IL-7 as key regulator of lymphatic vessel expansion in TLS. Indeed prophylactic block with IL-7 affects LEC proliferation, determining the formation of lymphatic vessels with smaller calibre. Whilst this defect is not complete it suggests a role for IL-7 in the early phases of TLS associated lymphangiogenesis.

During ontogeny, LTβR triggering has been also shown to activate surrounding stromal cells to produce VEGF-C, a crucial mediator of lymphangiogenesis (11). In our system, genetic deletion of LTβR results in a reduction of lymphatic vessel number and size and a significant reduction in VEGF-C transcript expression post cannulation. Treatment of *LtβR-/-* mice with recombinant VEGF-C was only partially able to restore the *LtβR-/-* defect suggesting a direct role for the latter in lymphatic vessel remodelling. Interestingly, blocking $LT\alpha_1\beta_2$ did not influence LEC proliferation, as expected, but rather decreased the complexity of the vascular network in the cannulated samples. Accordingly, it has been previously shown that blocking VEGF receptor signalling can inhibit the formation of complex tube of umbilical vein endothelial cells and LECs (41–43).

Previous studies have indicated a role for lymphocytes in lymphangiogenesis (33, 40, 44–46). In our model, the second phase of expansion of the lymphatic vessels is similarly affected by lack of $LT\alpha_1\beta_2$ and Rorγt+ cells. We demonstrated that *Rorc-/-* mice, while forming normal TLS (data not shown) are characterised by a significant defect in lymphatic

vessel expansion, similar to that observed in the *LtβR-/-* mice. This, associated with the defect in $LT\alpha_1\beta_2$ observed in the *Rorc-/-* mice suggests that Rorγt+ represent a critical source of $LT\alpha_1\beta_2$ during TLS formation. While the role of adult LTi in TLS formation is still debated, the role of Rorγt+ Th17 in TLS establishment and chemokine expression at ectopic sites is well recognised(47, 48). Here we suggest that Rorγt+ cells, providing $LT\alpha_1\beta_2$ play a larger and more complex role within TLS regulating their homeostatic resolution in the tissue.

Interestingly the defect observed in the lymphatic vessels in absence of mature lymphocytes is already present in the early phases of TLS establishment, in a phase that is independent from LTβR activity. The decrease in IL-7 transcript observed in the *Rag2-/-* mice could justify this defective phenotype and deserves further investigations (Suppl fig 3).

Lymphocyte derived $LT\alpha_1\beta_2$ is important for the full acquisition of lymphoid features by the TLS and has therefore been identified as a suitable target for TLS associated disease (15, 49). Unfortunately, clinical trials which block the lymphotoxin pathway in rheumatoid arthritis failed to meet primary end points, thus suggesting a more complex or redundant role for this molecule in the system (50). Our data support a critical for $LT\alpha_1\beta_2$ in TLS associated lymphoneogenesis and provide a potential explanation as to why blocking the lymphotoxin pathway in TLS associated diseases may not be effective based on a requirement for the expansion lymphatic vessels to enable lymphocyte egress during the resolution phase of inflammation.

Supplementary Material

Refer to Web version on PubMed Central for supplementary material.

Acknowledgments

We are grateful to the personnel in BMSU for taking care of our animal colonies. We are indebted to Klaus Pfeffer for proving *Ltbr*$^{-/-}$ mice, and to Prof. Peter Lane for providing *Rorc*$^{-/-}$ mice. This work was funded by Wellcome Trust, FB holds an ARUK Senior Fellowship, HMG holds an ARUK Career development Fellowship (19899). CB is recipient of ARUK program grant. FB, HMG and CB are part of the ARUK Centre of Excellence for the Pathogenesis of Rheumatoid Arthritis.

Funding: FB was funded by Wellcome Trust.

References

1. Acton SE, Farrugia AJ, Astarita JL, Mourao-Sa D, Jenkins RP, Nye E, Hooper S, van Blijswijk J, Rogers NC, Snelgrove KJ, Rosewell I, et al. Dendritic cells control fibroblastic reticular network tension and lymph node expansion. Nature. 2014; 514:498–502. [PubMed: 25341788]
2. Liao S, Ruddle NH. Synchrony of high endothelial venules and lymphatic vessels revealed by immunization. J Immunol. 2006; 177:3369–3379. [PubMed: 16920978]
3. Kim H, Kataru RP, Koh GY. Regulation and implications of inflammatory lymphangiogenesis. Trends in immunology. 2012; 33:350–356. [PubMed: 22579522]
4. Huggenberger R, Siddiqui SS, Brander D, Ullmann S, Zimmermann K, Antsiferova M, Werner S, Alitalo K, Detmar M. An important role of lymphatic vessel activation in limiting acute inflammation. Blood. 2011; 117:4667–4678. [PubMed: 21364190]

5. Kataru RP, Jung K, Jang C, Yang H, Schwendener RA, Baik JE, Han SH, Alitalo K, Koh GY. Critical role of CD11b+ macrophages and VEGF in inflammatory lymphangiogenesis, antigen clearance, and inflammation resolution. Blood. 2009; 113:5650–5659. [PubMed: 19346498]
6. Polzer K, Baeten D, Soleiman A, Distler J, Gerlag DM, Tak PP, Schett G, Zwerina J. Tumour necrosis factor blockade increases lymphangiogenesis in murine and human arthritic joints. Annals of the rheumatic diseases. 2008; 67:1610–1616. [PubMed: 18174217]
7. Baluk P, Tammela T, Ator E, Lyubynska N, Achen MG, Hicklin DJ, Jeltsch M, Petrova TV, Pytowski B, Stacker SA, Yla-Herttuala S, et al. Pathogenesis of persistent lymphatic vessel hyperplasia in chronic airway inflammation. The Journal of clinical investigation. 2005; 115:247–257. [PubMed: 15668734]
8. Onder L, Narang P, Scandella E, Chai Q, Iolyeva M, Hoorweg K, Halin C, Richie E, Kaye P, Westermann J, Cupedo T, et al. IL-7-producing stromal cells are critical for lymph node remodeling. Blood. 2012; 120:4675–4683. [PubMed: 22955921]
9. Iolyeva M, Aebischer D, Proulx ST, Willrodt AH, Ecoiffier T, Haner S, Bouchaud G, Krieg C, Onder L, Ludewig B, Santambrogio L, et al. Interleukin-7 is produced by afferent lymphatic vessels and supports lymphatic drainage. Blood. 2013; 122:2271–2281. [PubMed: 23963040]
10. Kumar V, Scandella E, Danuser R, Onder L, Nitschke M, Fukui Y, Halin C, Ludewig B, Stein JV. Global lymphoid tissue remodeling during a viral infection is orchestrated by a B cell-lymphotoxin-dependent pathway. Blood. 2010; 115:4725–4733. [PubMed: 20185585]
11. Vondenhoff MF, Greuter M, Goverse G, Elewaut D, Dewint P, Ware CF, Hoorweg K, Kraal G, Mebius RE. LT R Signaling Induces Cytokine Expression and Up-Regulates Lymphangiogenic Factors in Lymph Node Anlagen. The Journal of Immunology. 2009; 182:5439–5445. [PubMed: 19380791]
12. Chyou S, Benahmed F, Chen J, Kumar V, Tian S, Lipp M, Lu TT. Coordinated regulation of lymph node vascular-stromal growth first by CD11c+ cells and then by T and B cells. Journal of immunology. 2011; 187:5558–5567.
13. Benezech C, Nayar S, Finney BA, Withers DR, Lowe K, Desanti GE, Marriott CL, Watson SP, Caamano JH, Buckley CD, Barone F. CLEC-2 is required for development and maintenance of lymph nodes. Blood. 2014; 123:3200–3207. [PubMed: 24532804]
14. Hendriks HR, Duijvestijn AM, Kraal G. Rapid decrease in lymphocyte adherence to high endothelial venules in lymph nodes deprived of afferent lymphatic vessels. European Journal of Immunology. 1987; 17:1691–1695. [PubMed: 3500859]
15. Aloisi F, Pujol-Borrell R. Lymphoid neogenesis in chronic inflammatory diseases. Nature reviews Immunology. 2006; 6:205–217.
16. Barone F, Bombardieri M, Manzo A, Blades MC, Morgan PR, Challacombe SJ, Valesini G, Pitzalis C. Association of CXCL13 and CCL21 expression with the progressive organization of lymphoid-like structures in Sjögren's syndrome. Arthritis & Rheumatism. 2005; 52:1773–1784. [PubMed: 15934082]
17. Manzo A, Bugatti S, Caporali R, Prevo R, Jackson DG, Uguccioni M, Buckley CD, Montecucco C, Pitzalis C. CCL21 Expression Pattern of Human Secondary Lymphoid Organ Stroma Is Conserved in Inflammatory Lesions with Lymphoid Neogenesis. The American journal of pathology. 2007; 171:1549–1562. [PubMed: 17982129]
18. Barone F, Bombardieri M, Rosado MM, Morgan PR, Challacombe SJ, De Vita S, Carsetti R, Spencer J, Valesini G, Pitzalis C. CXCL13, CCL21, and CXCL12 expression in salivary glands of patients with Sjogren's syndrome and MALT lymphoma: association with reactive and malignant areas of lymphoid organization. J Immunol. 2008; 180:5130–5140. [PubMed: 18354239]
19. Barone F, Bombardieri M, Manzo A, Blades MC, Morgan PR, Challacombe SJ, Valesini G, Pitzalis C. Association of CXCL13 and CCL21 expression with the progressive organization of lymphoid-like structures in Sjogren's syndrome. Arthritis and rheumatism. 2005; 52:1773–1784. [PubMed: 15934082]
20. Pitzalis C, Jones GW, Bombardieri M, Jones SA. Ectopic lymphoid-like structures in infection, cancer and autoimmunity. Nature reviews Immunology. 2014; 14:447–462.

21. Peduto L, Dulauroy S, Lochner M, Spath GF, Morales MA, Cumano A, Eberl G. Inflammation Recapitulates the Ontogeny of Lymphoid Stromal Cells. The Journal of Immunology. 2009; 182:5789–5799. [PubMed: 19380827]
22. Link A, Hardie DL, Favre S, Britschgi MR, Adams DH, Sixt M, Cyster JG, Buckley CD, Luther SA. Association of T-Zone Reticular Networks and Conduits with Ectopic Lymphoid Tissues in Mice and Humans. The American journal of pathology. 2011; 178:1662–1675. [PubMed: 21435450]
23. Meier D, Bornmann C, Chappaz S, Schmutz S, Otten LA, Ceredig R, Acha-Orbea H, Finke D. Ectopic lymphoid-organ development occurs through interleukin 7-mediated enhanced survival of lymphoid-tissue-inducer cells. Immunity. 2007; 26:643–654. [PubMed: 17521585]
24. Cupedo T, Jansen W, Kraal G, Mebius RE. Induction of Secondary and Tertiary Lymphoid Structures in the Skin. Immunity. 2004; 21:655–667. [PubMed: 15539152]
25. Luther SA, Lopez T, Bai W, Hanahan D, Cyster JG. BLC expression in pancreatic islets causes B cell recruitment and lymphotoxin-dependent lymphoid neogenesis. Immunity. 2000; 12:471–481. [PubMed: 10843380]
26. Barone F, Nayar S, Campos J, Cloake T, Withers DR, Toellner KM, Zhang Y, Fouser L, Fisher B, Bowman S, Rangel-Moreno J, et al. IL-22 regulates lymphoid chemokine production and assembly of tertiary lymphoid organs. Proceedings of the National Academy of Sciences of the United States of America. 2015; 112:11024–11029. [PubMed: 26286991]
27. Klimiuk PA, Sierakowski S, Latosiewicz R, Cylwik B, Skowronski J, Chwiecko J. Serum matrix metalloproteinases and tissue inhibitors of metalloproteinases in different histological variants of rheumatoid synovitis. Rheumatology. 2002; 41:78–87. [PubMed: 11792884]
28. Link A, Vogt TK, Favre S, Britschgi MR, Acha-Orbea H, Hinz B, Cyster JG, Luther SA. Fibroblastic reticular cells in lymph nodes regulate the homeostasis of naive T cells. Nature immunology. 2007; 8:1255–1265. [PubMed: 17893676]
29. Bombardieri M, Barone F, Lucchesi D, Nayar S, van den Berg WB, Proctor G, Buckley CD, Pitzalis C. Inducible tertiary lymphoid structures, autoimmunity, and exocrine dysfunction in a novel model of salivary gland inflammation in C57BL/6 mice. J Immunol. 2012; 189:3767–3776. [PubMed: 22942425]
30. De Togni P, Goellner J, Ruddle NH, Streeter PR, Fick A, Mariathasan S, Smith SC, Carlson R, Shornick LP, Strauss-Schoenberger J, et al. Abnormal development of peripheral lymphoid organs in mice deficient in lymphotoxin. Science. 1994; 264:703–707. [PubMed: 8171322]
31. Mebius RE. Organogenesis of lymphoid tissues. Nature Reviews Immunology. 2003; 3:292–303.
32. Eberl G, Marmon S, Sunshine MJ, Rennert PD, Choi Y, Littman DR. An essential function for the nuclear receptor RORgamma(t) in the generation of fetal lymphoid tissue inducer cells. Nature immunology. 2004; 5:64–73. [PubMed: 14691482]
33. Liao S, Ruddle NH. Synchrony of high endothelial venules and lymphatic vessels revealed by immunization. Journal of immunology. 2006; 177:3369–3379.
34. Pitzalis C, Jones GW, Bombardieri M, Jones SA. Ectopic lymphoid-like structures in infection, cancer and autoimmunity. Nature reviews Immunology. 2014; 14:447–462.
35. Carragher DM, Rangel-Moreno J, Randall TD. Ectopic lymphoid tissues and local immunity. Seminars in immunology. 2008; 20:26–42. [PubMed: 18243731]
36. Kim H, Kataru RP, Koh GY. Inflammation-associated lymphangiogenesis: a double-edged sword? The Journal of clinical investigation. 2014; 124:936–942. [PubMed: 24590279]
37. Thaunat O, Kerjaschki D, Nicoletti A. Is defective lymphatic drainage a trigger for lymphoid neogenesis? Trends in immunology. 2006; 27:441–445. [PubMed: 16920402]
38. Ruddle NH. Lymphatic vessels and tertiary lymphoid organs. The Journal of clinical investigation. 2014; 124:953–959. [PubMed: 24590281]
39. Rangel-Moreno J, Moyron-Quiroz JE, Carragher DM, Kusser K, Hartson L, Moquin A, Randall TD. Omental milky spots develop in the absence of lymphoid tissue-inducer cells and support B and T cell responses to peritoneal antigens. Immunity. 2009; 30:731–743. [PubMed: 19427241]
40. Furtado GC, Marinkovic T, Martin AP, Garin A, Hoch B, Hubner W, Chen BK, Genden E, Skobe M, Lira SA. Lymphotoxin beta receptor signaling is required for inflammatory lymphangiogenesis in the thyroid. Proc Natl Acad Sci U S A. 2007; 104:5026–5031. [PubMed: 17360402]

41. Kajiya K, Sawane M, Huggenberger R, Detmar M. Activation of the VEGFR-3 pathway by VEGF-C attenuates UVB-induced edema formation and skin inflammation by promoting lymphangiogenesis. The Journal of investigative dermatology. 2009; 129:1292–1298. [PubMed: 19005491]

42. Halin C, Fahrngruber H, Meingassner JG, Bold G, Littlewood-Evans A, Stuetz A, Detmar M. Inhibition of chronic and acute skin inflammation by treatment with a vascular endothelial growth factor receptor tyrosine kinase inhibitor. The American Journal of Pathology. 2008; 173:265–277. [PubMed: 18535184]

43. Hagura A, Asai J, Maruyama K, Takenaka H, Kinoshita S, Katoh N. The VEGF-C/VEGFR3 signaling pathway contributes to resolving chronic skin inflammation by activating lymphatic vessel function. Journal of dermatological science. 2014; 73:135–141. [PubMed: 24252749]

44. Armengol MP, Juan M, Lucas-Martin A, Fernandez-Figueras MT, Jaraquemada D, Gallart T, Pujol-Borrell R. Thyroid autoimmune disease: demonstration of thyroid antigen-specific B cells and recombination-activating gene expression in chemokine-containing active intrathyroidal germinal centers. The American journal of pathology. 2001; 159:861–873. [PubMed: 11549579]

45. Klimiuk PA, Sierakowski S, Latosiewicz R, Cylwik JP, Cylwik B, Skowronski J, Chwiecko J. Circulating tumour necrosis factor alpha and soluble tumour necrosis factor receptors in patients with different patterns of rheumatoid synovitis. Annals of the rheumatic diseases. 2003; 62:472–475. [PubMed: 12695163]

46. Klimiuk PA, Sierakowski S, Latosiewicz R, Cylwik JP, Cylwik B, Skowronski J, Chwiecko J. Interleukin-6, soluble interleukin-2 receptor and soluble interleukin-6 receptor in the sera of patients with different histological patterns of rheumatoid synovitis. Clinical and experimental rheumatology. 2003; 21:63–69. [PubMed: 12673891]

47. Grogan JL, Ouyang W. A role for Th17 cells in the regulation of tertiary lymphoid follicles. European journal of immunology. 2012; 42:2255–2262. [PubMed: 22949324]

48. Peters A, Pitcher LA, Sullivan JM, Mitsdoerffer M, Acton SE, Franz B, Wucherpfennig K, Turley S, Carroll MC, Sobel RA, Bettelli E, et al. Th17 cells induce ectopic lymphoid follicles in central nervous system tissue inflammation. Immunity. 2011; 35:986–996. [PubMed: 22177922]

49. Marinkovic T. Interaction of mature CD3+CD4+ T cells with dendritic cells triggers the development of tertiary lymphoid structures in the thyroid. Journal of Clinical Investigation. 2006; 116:2622–2632. [PubMed: 16998590]

50. Genovese MC, Maria WG, Alloway Jeff A, Andrew R Baldassare, Chase Walter, Newman Charlotte, Weaver Megan L. Efficacy and Safety of Baminercept in the Treatment of Rheumatoid Arthritis (RA) Results of the Phase 2B Study in the TNF-IR Population. Arthritis & Rheumatism. 2009:60.

Europe PMC Funders Author Manuscripts

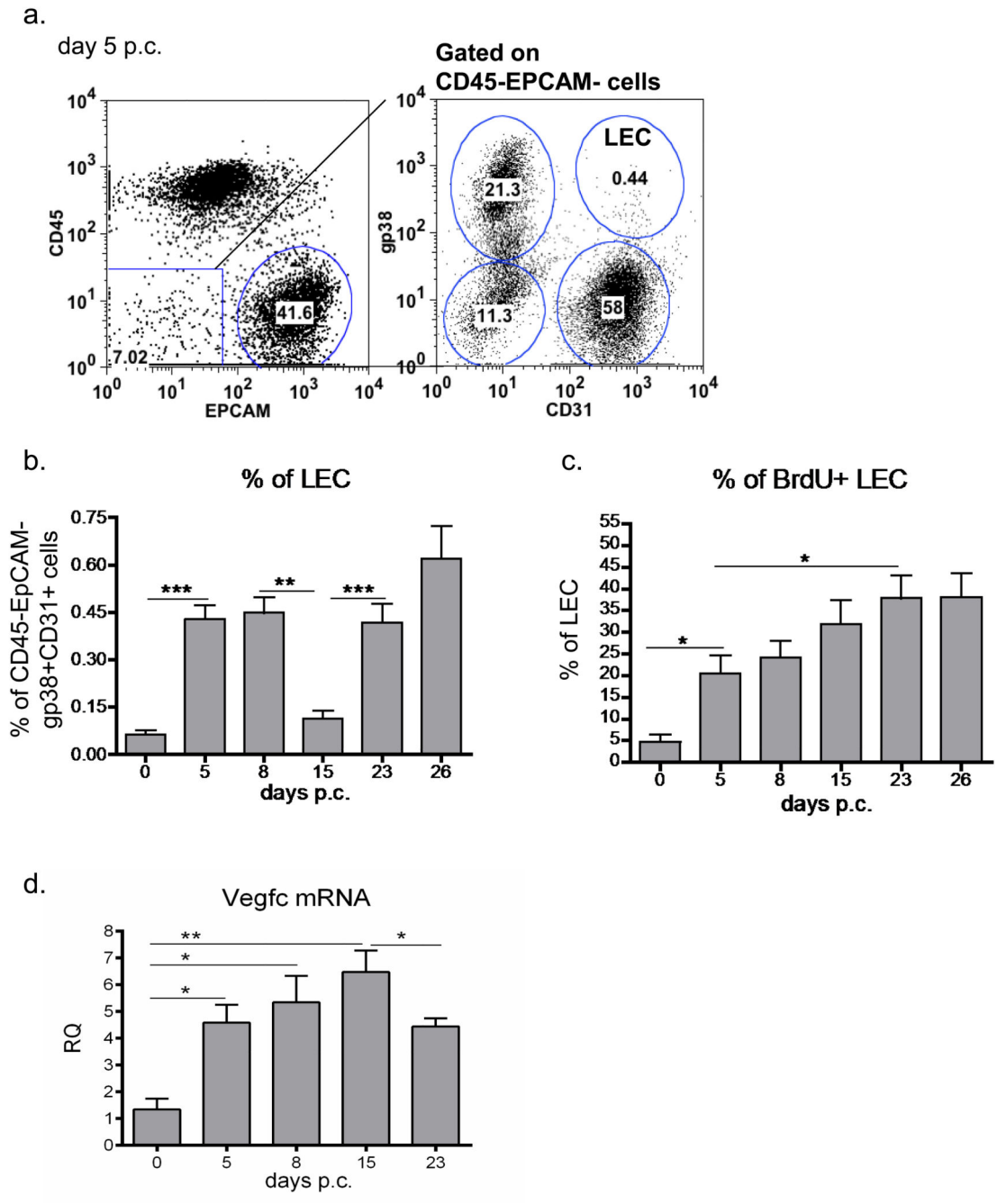

Figure 1. Bimodal expansion of the lymphatic bed during TLS development.

a, Representative dot plots showing flow cytometry staining for gp38, CD31 in the CD45-EPCAM- cells from salivary glands isolated at day 5 post viral cannulation (p.c.). The lymphatic endothelial cells (LECs) are identified as gp38+CD31+ cells. **b,** Time course of LEC expansion during the inflammatory process determined by flow cytometry (percentage of gp38+CD31+ population in the CD45-EPCAM- component) from infected WT mice at day 0, day 5, day 8, day 15, day 23, day 26 p.c. Data presented as means of five independent experiments ** $p < 0.01$; ***, $p < 0.001$, unpaired t test, comparing LEC population at each

time point with day 0 p.c. LEC. **c,** Graphs showing summary of analysis for percentage of proliferating (BrdU+) gp38+CD31+ LEC in the CD45-EPCAM- stromal fraction. BrdU administred from day 0 continuously *, $p < 0.05$, ** $p < 0.01$ versus day 0 p.c. WT mice. **d,** Quantitative RT-PCR analysis of mRNA transcript for Vegfc in *wt* mice at day 0, day 5, 8, 15 and 23 p.c. Transcripts were normalized to housekeeping gene β-actin. The relative expression values (RQ) were calibrated with day 0 p.c. salivary gland values; *, $p < 0.05$, **, $p < 0.01$. Data are representative mean+s.e.m of three to four experiments with six to four glands analysed per group. Data are representative of three to four independent experiments with six to eight glands analysed per group. Data shown as mean+s.e.m.

Europe PMC Funders Author Manuscripts

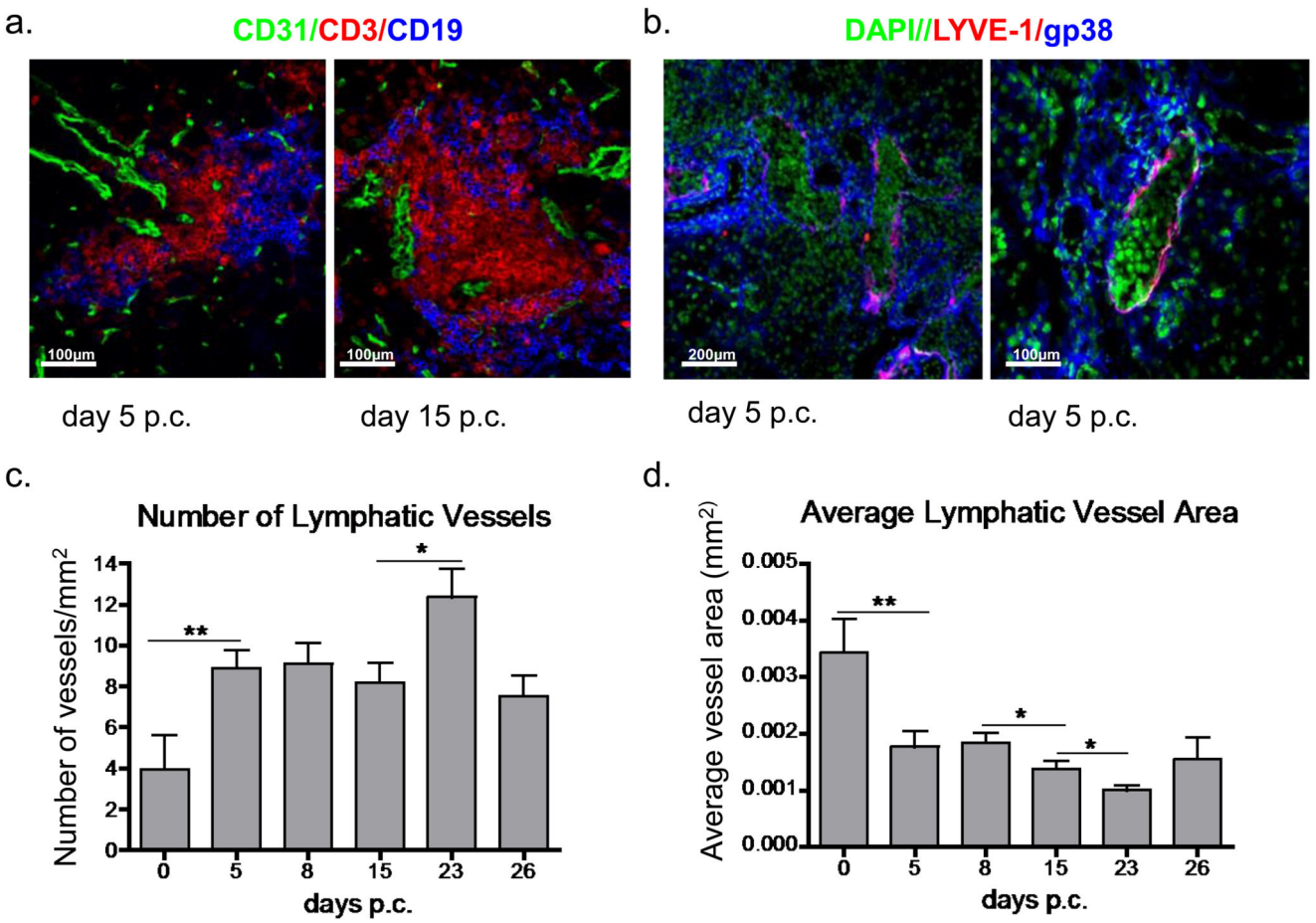

Figure 2. Remodelling of the lymphatic network during TLS development.

a, Microphotograph of lymphoid aggregates from infected salivary glands (day 5 and 15 p.c.) from *wt* mice stained for CD3 (red), CD19 (blue) and CD31 (green). Original magnifications 25X. **b,** Microphotograph of lymphatic vessels in infected salivary glands (day 5 p.c.) from *wt* mice stained for LYVE-1 (red), gp38 (blue) and DAPI (green). Original magnifications 10X and 25X. **c-d,** Graphs summarizing image analysis in salivary gland tissue sections at different time-points of the inflammatory process to identify changes observed in lymphatic vessel expansion. The graphs in show the number of lymphatic vessels per mm^2 of tissue area **(c)** and average vessel area; expressed in mm^2 **(d)** *, $p < 0.05$, ** $p < 0.01$ versus day 0 p.c. WT mice. Data are representative of three to four independent experiments with four to six glands analysed per group. Data shown as mean+s.e.m.

Europe PMC Funders Author Manuscripts

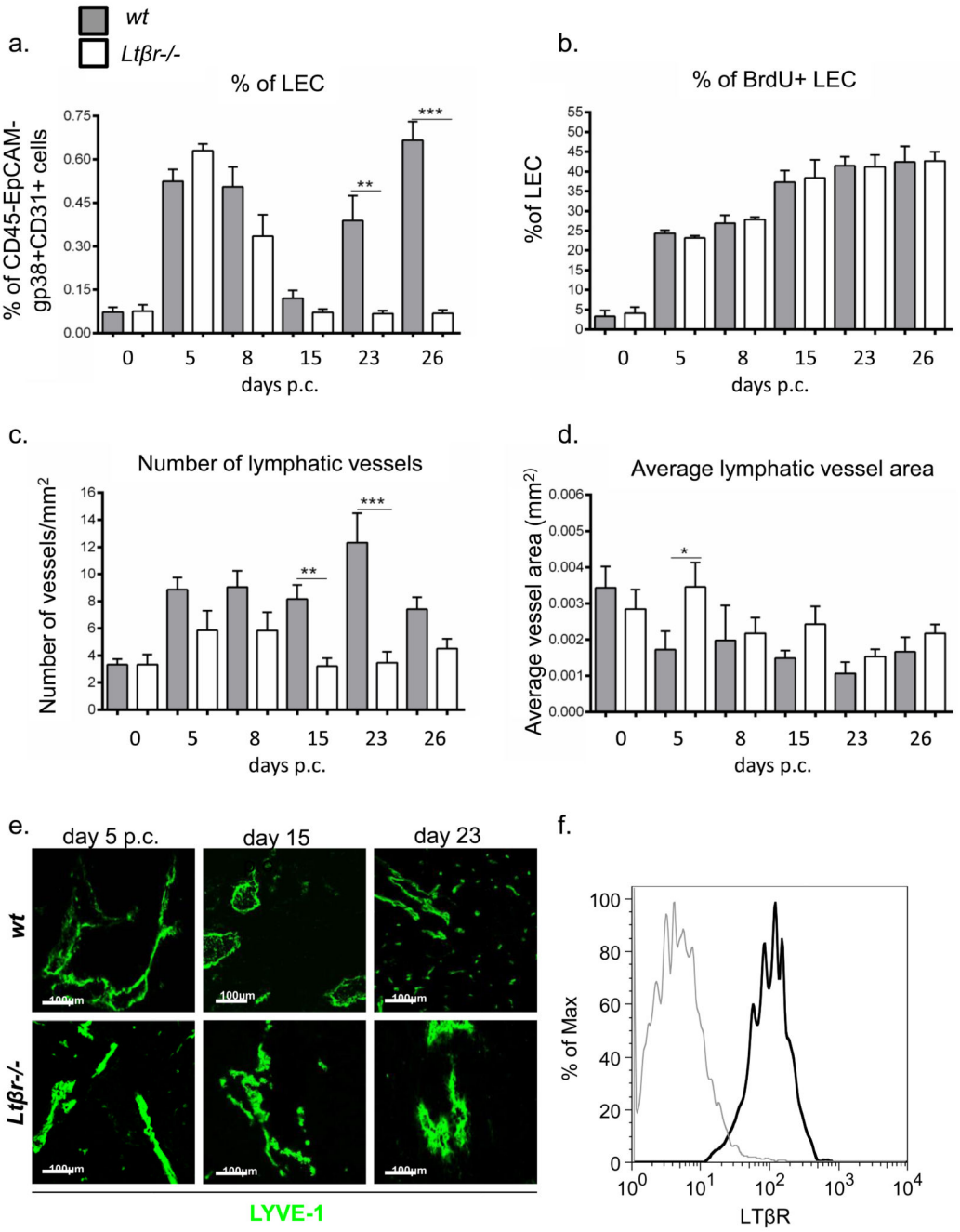

Figure 3. Lack of LTβ affects lymphangiogenesis in TLS

a, Graph showing flow cytometry analysis of LEC expansion in *wt* mice (grey bars) compared to *LtβR-/-* (white bars) mice. *, $p < 0.05$, **, $p < 0.01$, unpaired t test, comparing gp38+CD31+ LEC population in infected *ko* mice at various time-points to their *wt* counterparts. **b,** Graphs showing summary of analysis for percentage of proliferating (BrdU +) gp38+CD31+ LEC within the CD45-EPCAM- stromal fraction in *wt* mice (grey bars) compared to *LtβR-/-* (white bars) mice. **c-d,** Summarizing image analysis results showing differences observed in the number of lymphatic vessels per mm^2 of tissue area **(c)** and

average vessel area (mm^2) **(d)** in *wt* mice (grey bars) compared to *ltβR-/-* mice (white bars). Data are representative of three independent experiments with four to six glands analysed per group. Data shown as mean+s.e.m *, $p < 0.05$; **, $p < 0.01$, ***, $p < 0.001$, unpaired t test, comparing LYVE-1+ vessels in infected *ko* mice at various time-points to their *wt* counterparts. **e,** Representative microphotograph of lymphatic vessels in infected salivary glands (day 5, day 15 and day 23 p.c.) from *ltβR-/-* mice in comparison to *wt* mice stained for LYVE-1 (green). Scale bar 100um. **f,** Histogram showing LTbR expression (black) and isotype control (grey) on LECs in salivary glands at day 5 p.c.

f, Quantitative RT-PCR analysis of mRNA transcript for Vegfc in *ltβR-/-* mice (white bars) in comparison to their *wt* counterparts (grey bars) at day 0, day 5, 8, 15 and 23 p.c. Transcripts were normalized to housekeeping gene β-actin. The relative expression values (RQ) were calibrated with day 0 p.c. salivary gland values; *, $p < 0.05$, **, $p < 0.01$ versus *wt* mice. Data are representative mean+s.e.m of three to four experiments with six to four glands analysed per group. Data represented as mean+s.e.m of two independent experiments, 6 to 8 glands evaluated/experiment.

Europe PMC Funders Author Manuscripts

Europe PMC Funders Author Manuscripts

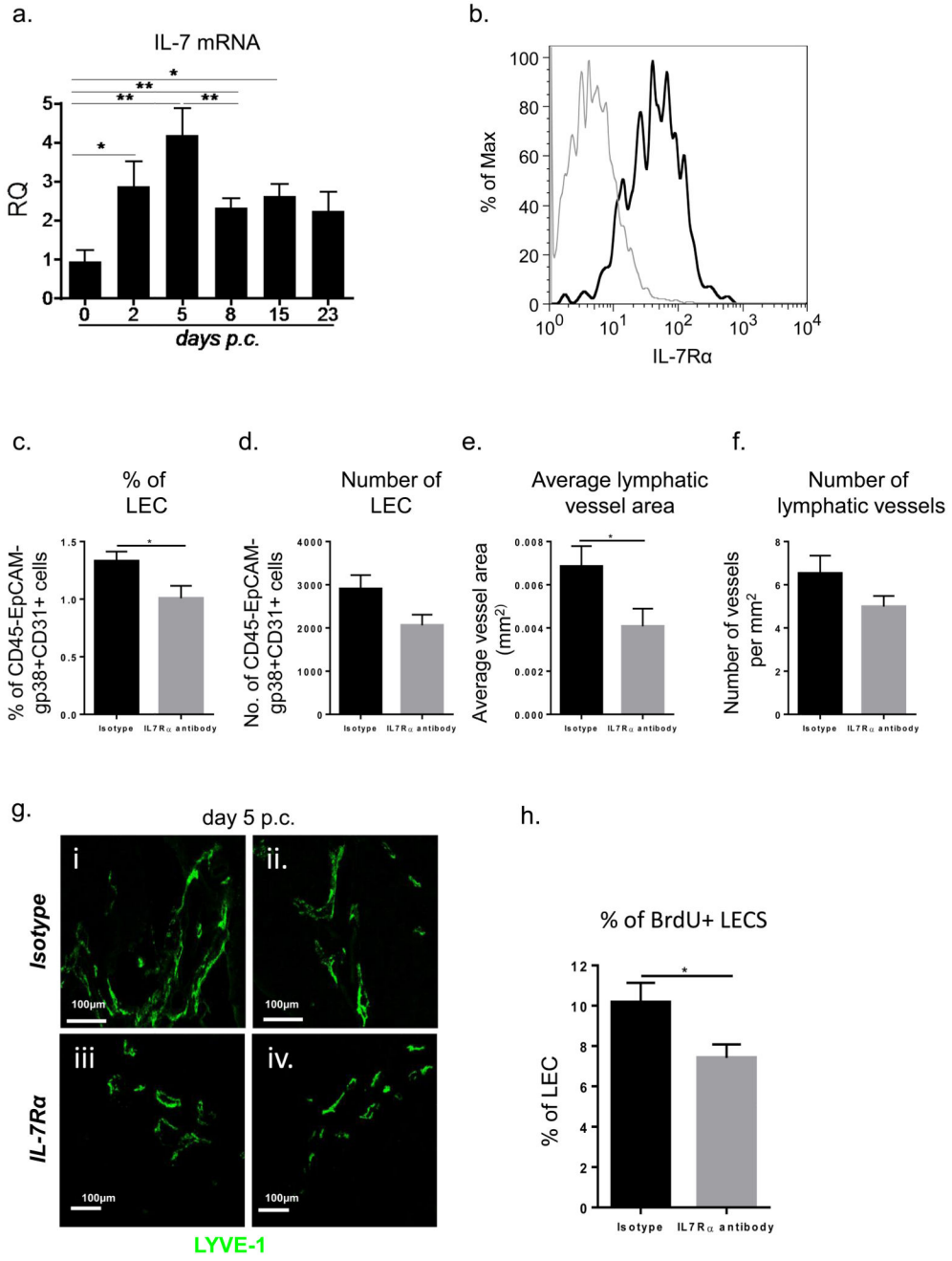

Figure 4. The early phase of lymphatic vessels remodelling is dependent on IL-7.

a, Quantitative RT-PCR analysis of mRNA transcript for il-7 in *wt* mice (white bars) in comparison to their *wt* counterparts (grey bars) at day 0, day 2, day 5, 8, 15 and 23 p.c. Transcripts were normalized to housekeeping gene pdgfrβ. The relative expression values (RQ) were calibrated with day 0 p.c. salivary gland values; *, $p < 0.05$, **, $p < 0.01$. Data are representative mean+s.e.m of three to four experiments with six to four glands analysed per group. **b,** Histogram showing IL-7Rα expression (black) and isotype control (grey) on LECs in salivary glands at day 5 p.c. **c,** Graph showing flow cytometry analysis of

percentage of LEC in *wt* mice treated with isotype antibody (black bars) as compared to IL-7Ra blocking antibody treated mice (grey bars) mice. Data represented as mean+s.e.m *, $p < 0.05$. **d,** Graph showing flow cytometry analysis of absolute number of LEC in *wt* mice treated with isotype antibody (black bars) as compared to IL-7Ra blocking antibody treated mice (grey bars) mice. Data represented as mean+s.e.m. **e-f,** Graphs summarizing image analysis results showing differences observed in the number of lymphatic vessels per mm^2 of tissue area and average vessel area (mm^2) in *wt* mice treated with IL7Rα blocking antibody (grey bars) compared to isotype treated mice (black bars). Data are representative of two independent experiments with four to six glands analysed per group. Data shown as mean+s.e.m *, $p < 0.05$; unpaired t test. **g,** Representative microphotograph of lymphatic vessels in infected salivary glands (day 5 p.c.) from IL7Rα blocking antibody treated mice in comparison to *wt* mice treated with isotype stained for LYVE-1 (green). Scale bar 100um. **h,** Graphs showing summary of analysis for percentage of proliferating (BrdU+) gp38+CD31+ LEC within the CD45-EPCAM- stromal fraction in *wt* mice treated with isotype antibody (black bars) as compared to IL-7Rα blocking antibody treated mice (grey bars) mice. Data represented as mean+s.e.m *, $p < 0.05$.

Europe PMC Funders Author Manuscripts

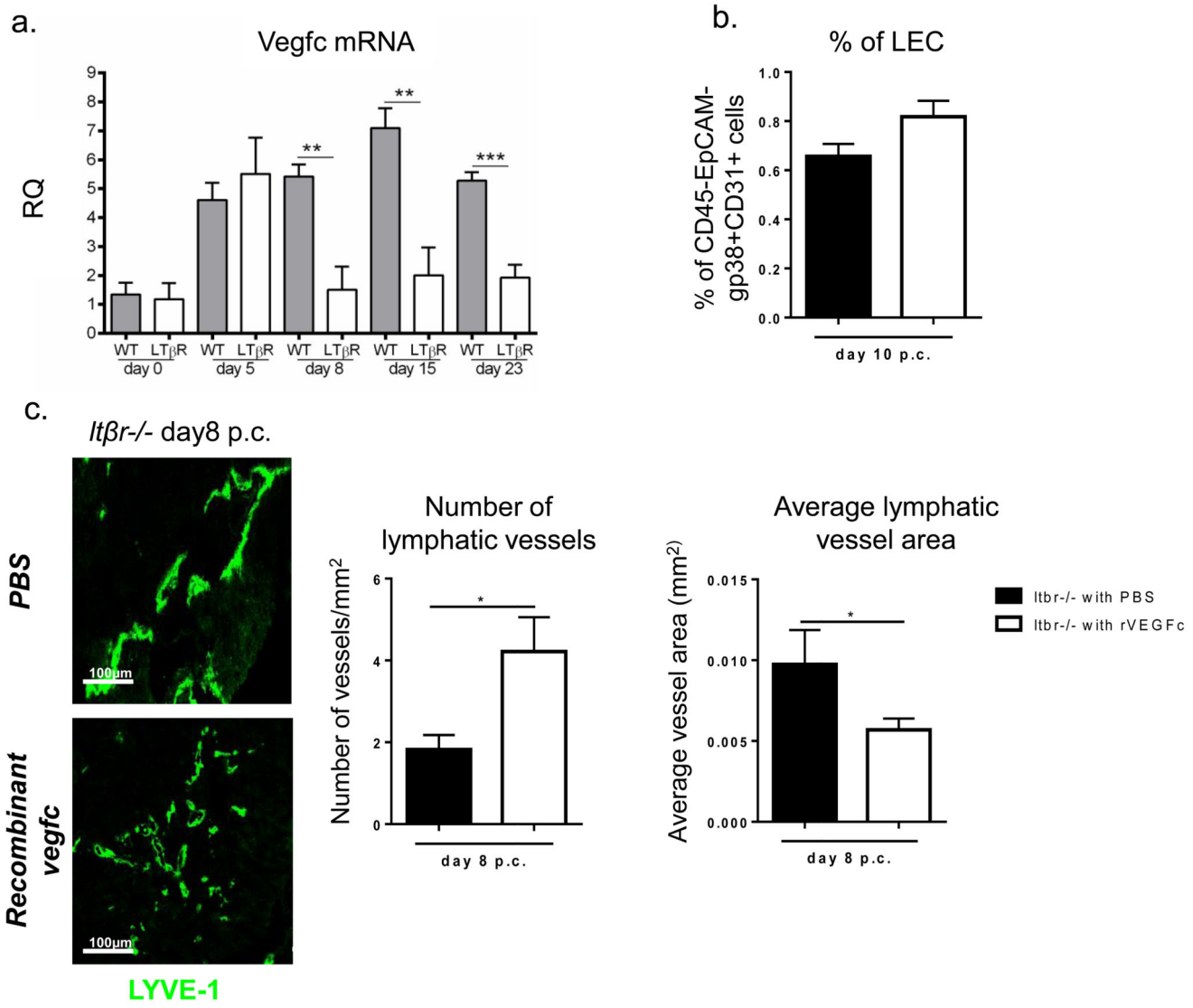

Figure 5. LTα$_1$β$_2$ induces the formation of complex lymphatic networks in vitro

a, Quantitative RT-PCR analysis of mRNA transcript for Vegfc in *ltβR-/-* mice (white bars) in comparison to their *wt* counterparts (grey bars) at day 0, day 5, 8, 15 and 23 p.c. Transcripts were normalized to housekeeping gene β-actin. The relative expression values (RQ) were calibrated with day 0 p.c. salivary gland values; *, $p < 0.05$, **, $p < 0.01$ versus *wt* mice. Data are representative mean+s.e.m of three to four experiments with six to four glands analysed per group. **b,** Graph showing flow cytometry analysis of percentage of LEC in *ltβR-/-* mice treated with recombinant vegfc (white bars) as compared to PBS treated mice (black bars) mice. Data represented as mean+s.e.m. **c,** Representative microphotograph of lymphatic vessels in infected salivary glands (day 8 p.c.) from recombinant vegfc treated mice in comparison to PBS treated *ltβR-/-* mice stained for LYVE-1 (green). Scale bar 100um. Summarizing image analysis results showing differences observed in the number of lymphatic vessels per mm^2 of tissue area and average vessel area (mm^2) in *ltβR-/-* mice treated with recombinant vegfc (white bars) as compared to PBS treated mice (black bars)

mice. Data are representative of two independent experiments with four to six glands analysed per group. Data shown as mean+s.e.m *, $p < 0.05$; unpaired t test.

Europe PMC Funders Author Manuscripts

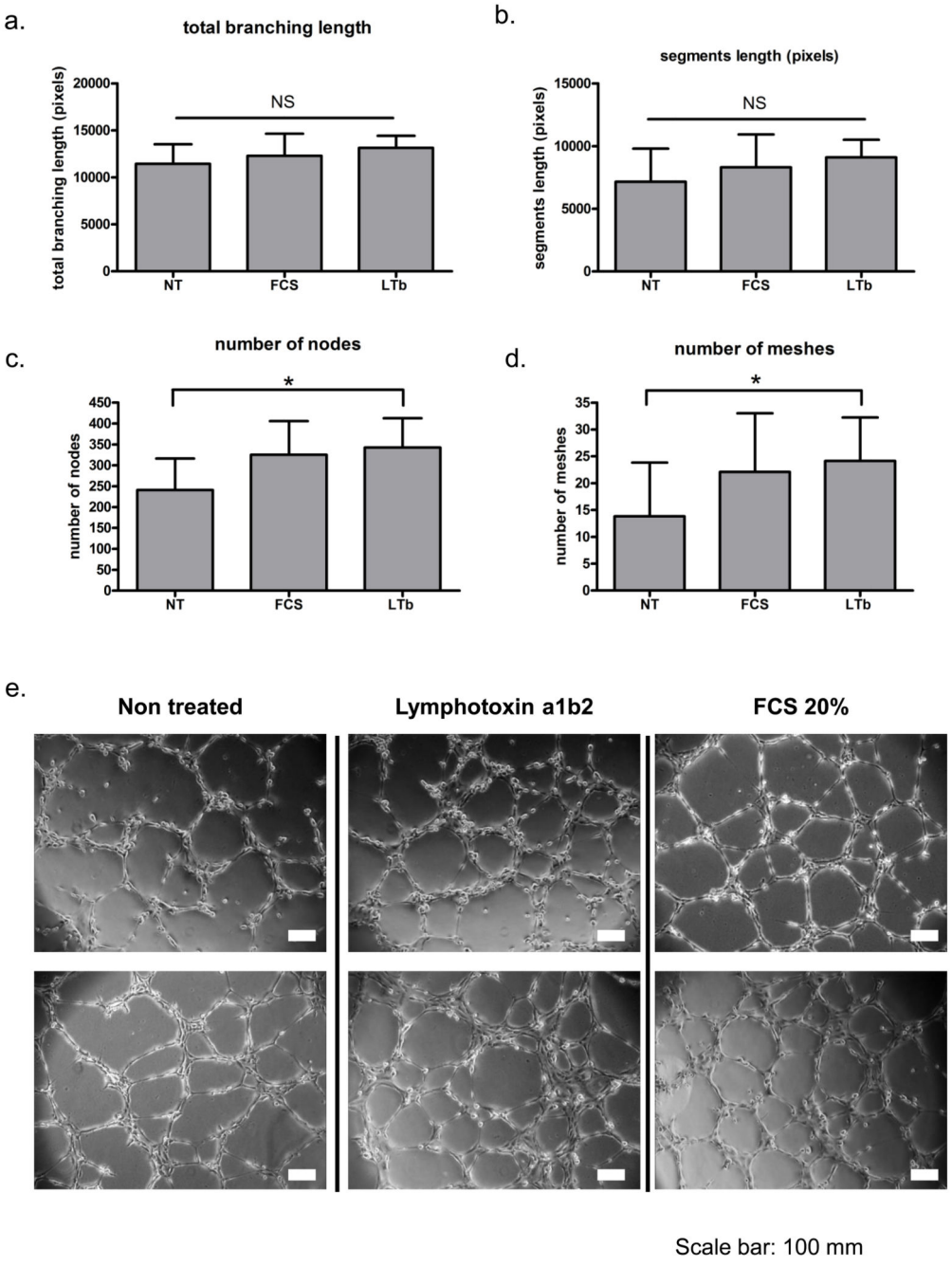

Figure 6. LTα$_1$β$_2$ induces the formation of complex lymphatic networks

In vitro analysis of the effect of LTα$_1$β$_2$ stimulation on lymphatic endothelial cell tube formation assay showing **a,** total branching length **b,** segment length (pixels) **c,** number of nodes and **d,** number of meshes. **e,** Representative microphotographs of non-treated (NT), FCS treated and LTα$_1$β$_2$ treated lymphatic endothelial cells. Data is representative of three independent experiments; * represents $p<0.05$ after 1 way repeated measurements ANOVA analysis. NS: non-significant differences found.

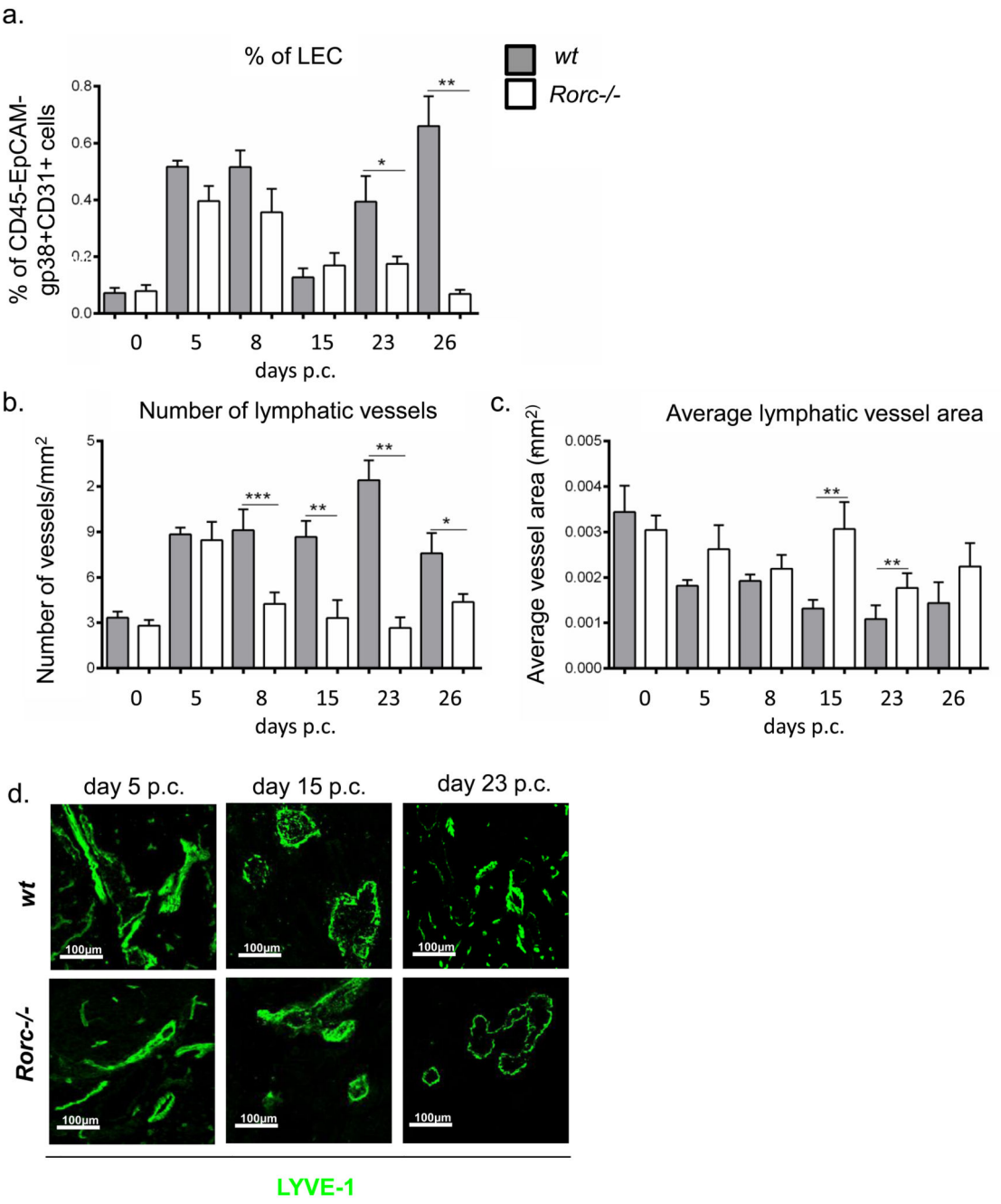

Figure 7. Lymphatic vessel formation is influenced by the expression of LTβ by Rorγ$^+$ cells.

a, Graph showing flow cytometry analysis of LEC expansion in *wt* mice (grey bars) compared to *rorγ-/-* mice (white bars). Data represented as mean+s.e.m of two independent experiments. *, $p < 0.05$, **, $p < 0.01$, unpaired t test, comparing gp38+CD31+ LEC population in infected *ko* mice at various time-points to their *wt* counterparts. **b,** Graphs showing the number of lymphatic vessels per mm^2 of tissue in *wt* mice (grey bars) compared to *Rorc-/-* (white bars) mice. Data are representative mean+s.e.m of three independent experiments with four to six glands analysed per group. *, $p < 0.05$; **, $p < 0.01$, ***, $p <$

Europe PMC Funders Author Manuscripts

0.001, unpaired t test, comparing LYVE-1+ vessels in infected *ko* mice at various time-points to their *wt* counterparts. **c,** Graphs showing average vessel area (mm^2) in *wt* mice (grey bars) compared to *Rorc-/-* mice (white bars). Data are representative mean+s.e.m of three independent experiments with four to six glands analysed per group. *, $p < 0.05$; **, $p < 0.01$, ***, $p < 0.001$, unpaired t test, comparing LYVE-1+ vessels in infected *ko* mice at various time-points to their *wt* counterparts. **d,** Representative microphotograph of lymphatic vessels in infected salivary glands (day 5, day 15 and day 23 p.c.) from *Rorc-/-* mice in comparison to *wt* mice stained for LYVE-1 (green). Scale bar 100um.

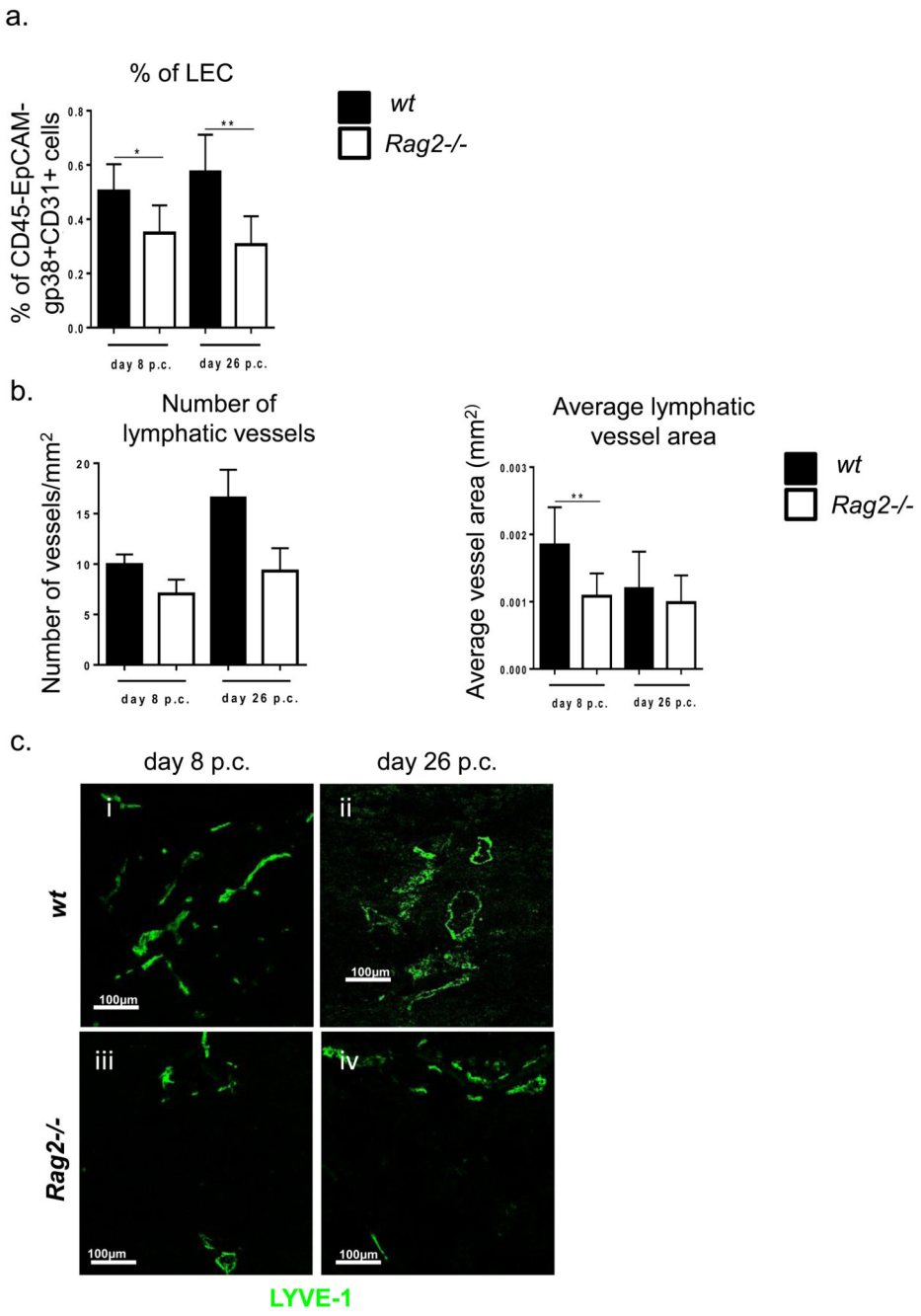

Figure 8. Lack of lymphocytes affect both phases of lymphatic vessel expansion.

a, Graph showing flow cytometry analysis of LEC expansion in *wt* mice (grey bars) compared to *rag-/-* mice (white bars) at day 8 and day 26 p.c. Data represented as mean +s.e.m of two independent experiments. *, $p < 0.05$, **, $p < 0.01$, unpaired t test, comparing gp38+CD31+ LEC population in infected *ko* mice at various time-points to their *wt* counterparts. **b,** Graphs showing number of lymphatic vessels and average vessel area (mm^2) in *wt* mice (black bars) compared to *rag-/-* mice (white bars). Data are representative mean +s.e.m of three independent experiments with four to six glands analysed per group. **, p <

Europe PMC Funders Author Manuscripts

0.01, unpaired t test, comparing LYVE-1+ vessels in infected *ko* mice at various time-points to their *wt* counterparts. **c,** Representative microphotograph of lymphatic vessels in infected salivary glands (day 8 and day 26 p.c.) from *rag-/-* mice in comparison to *wt* mice stained for LYVE-1 (green). Scale bar 100um.

Europe PMC Funders Author Manuscripts